Research article

Han Yao, Fan Shi, Zhaoyang Wu, Xinzhu Xu, Teng Wang, Xiaomin Liu, Peng Xi, Fufei Pang
and Xianglong Zeng*

A mode generator and multiplexer at visible wavelength based on all-fiber mode selective coupler

Abstract: Using an all-fiber mode selective coupler (MSC) at the visible band, here we experimentally demonstrate a generating and wavelength multiplexing scheme for the cylindrical vector (CV) and vortex beams (VBs). The proposed MSCs act as efficient mode converters to produce spectrally insensitive high-order modes (HOMs) at the wavelength ranging from 450 to 980 nm, which have broad operation bandwidth (more than 7 nm), high mode conversion efficiency (94%), and purity (98%), and low insert loss (below 0.5 dB). By adjusting the polarization state and the phase shift of linear polarization $(LP)_{11}$ mode respectively, the donut-shaped CVs and circular-polarization VBs are achieved. The focused intensity distribution of the donut beam on the cross- and axial-sections is monitored by using a confocal system. The all-fiber solution of producing and multiplexing HOMs opens a new route for stimulated emission depletion microscopy applications.

*Corresponding author: Xianglong Zeng, Key Laboratory of Specialty Fiber Optics and Optical Access Networks, Joint International Research Laboratory of Specialty Fiber Optics and Advanced Communication, Shanghai Institute for Advanced Communication and Data Science, Shanghai University, Shanghai 200444, P.R. China, e-mail: zenglong@shu.edu.cn. https://orcid.org/0000-0001-7817-173X
Han Yao, Fan Shi, Teng Wang and Fufei Pang: Key Laboratory of Specialty Fiber Optics and Optical Access Networks, Joint International Research Laboratory of Specialty Fiber Optics and Advanced Communication, Shanghai Institute for Advanced Communication and Data Science, Shanghai University, Shanghai 200444, P.R. China. https://orcid.org/0000-0003-2909-8163 (H. Yao); https://orcid.org/0000-0002-7106-4584 (F. Pang)
Zhaoyang Wu, Xinzhu Xu and Peng Xi: Department of Biomedical Engineering, College of Engineering, Peking University, Beijing 100871, P.R. China
Xiaomin Liu: Max Planck Institute for Polymer Research, 55128 Mainz, Germany

1 Introduction

Orthogonal multiplexing technology of high-order modes (HOMs) transmitted in few-mode fiber (FMF) has surpassed the capacity barrier in the traditional single mode fiber (SMF) communication system and provided the possibility for further exploring the freedom degrees of light beams, such as amplitude, phase, wavelength, and polarization [1–4]. Additionally, the HOMs have extensive transmission transverse area than the fundamental mode, more available energy of dispersion management and phase matching can be provided. Therefore, the HOMs play an important role in the research of 1.0 and 1.55-μm ultrafast fiber lasers [5–9]. The HOMs of visible band have been successfully applied in the fiber laser [10, 11], underwater wireless optical communication [12], and data encoding and decoding [13]. Moreover, the visible HOMs can be researched for stimulated emission depletion (STED) microscopy, and have provided nanoscale resolution to visualize the complex details of subcellular structure [14–16].

The degenerated HOMs transmitted in fiber include linear polarization $(LP)_{11}$, LP_{21}, LP_{02}, LP_{31}, and even higher order modes. They are composed of eigenmodes which can be stably transmitted in fiber. The LP_{11} mode is one of the most widely studied HOMs, which has four vector eigenmodes. These vector beams with axially symmetric polarization and circular intensity distribution in the cross-section are also called cylindrical vector beams (CVBs) [17]. In particular, the optical vortex beam (OVB) characterized by the helical wavefront can be generated by combining two orthogonal vector modes [18]. These beams with special polarization state and phase characteristic have significant applications, such as high-resolution measurement [19], particle trapping and manipulation [20], remote sensing technology [21, 22], etc.

So far, the HOMs generation technology, including free-space and all-fiber methods, is extremely mature for near-infrared wavelengths [18, 23–25]. The visible HOMs are mostly generated by employing free-space beam shaping devices [13, 15, 26], Al gratings [27], and holograms [28] at the desired wavelengths. It is a challenge to spatially precisely align the beams using the traditional free-space optical method, which usually leads to poor repeatability and stability. Additionally, the free-space devices, such as vortex phase plate, phase modulation module, and spatial light modulator, are bulk optics and typically designed for a specific wavelength. While the all-fiber method has more outstanding advantages, such as compactness, stability, and low cost. Therefore, the all-fiber HOMs solution in the visible band is of great significance. Recently, Zou et al. demonstrated an all-fiber laser with the direct generation of 635 nm HOM, and the OVB is generated by misaligning the cores of the FMF and the Pr^{3+}/Yb^{3+}-codoped ZrF_4-BaF_2-LaF_3-AlF_3-NaF (ZBLAN) fiber [10]. However, a large energy loss was introduced to the fiber laser based on the method, reducing the mode conversion and laser cavity oscillating efficiency. Zhang et al. proposed a scheme to generate 532 nm HOMs in a FMF via cascaded acoustically induced fiber gratings (AIFG) [29]. Yan et al. designed a configuration in which by using a long period fiber grating (LPFG), the fundamental mode can be converted to a donut beam for STED microscope [16]. Conversion bandwidth of the mentioned fiber gratings usually covers a few nanometers, leading to a narrow operating bandwidth of HOMs. Moreover, the central wavelength of the fiber gratings is easily influenced by environmental temperature and micro-curvature.

In this paper, we experimentally demonstrate an all-fiber scheme for generating HOMs and wavelength multiplexing at visible band based on a mode selective coupler (MSC). The proposed all-fiber MSC can convert the fundamental mode to donut-shaped mode in fiber. The MSC not only functions as a mode converter for producing HOMs, but also functions as a wavelength division multiplexer (WDM) for combining donut and Gaussian beams. The focused intensity distribution at focus is also measured based on a confocal microscope system to verify the possibility that the MSC provides an optical source for STED microscopy in the form of high integration and compactness. To our best knowledge, this is the first report that the MSC acts as an all-fiber mode generator and multiplexer at visible wavelength and can be potentially applied in STED microscopy.

2 Visible MSCs fabrication and performance evaluation

The schematic of the MSC is shown in Figure 1A. The MSC is composed of a SMF and a FMF (core/cladding diameter = 10/125 μm, NA = 0.23), which are fused together by using hydrogen oxygen flame technology to keep two fiber cores close to each other, so that light energy can be effectively transferred reciprocally. The claddings of two fibers are partly fused together to form a bi-conical shape, as shown in the inset of top- and cross-sectional coupling region. In addition, to avoid the perturbation of the external environment, the fused MSC is hermetically packaged inside U-type glass base plate and sealed in a heat shrink tube. The LP_{01} mode is launched into the SMF (pink) input port, if phase match condition is satisfied, fiber mode transformation is achieved in the coupling region. The degenerated LP_{11} mode can be excited at the FMF output port, while residual energy is output from the SMF output port. LP_{11} mode consists of four vector modes:
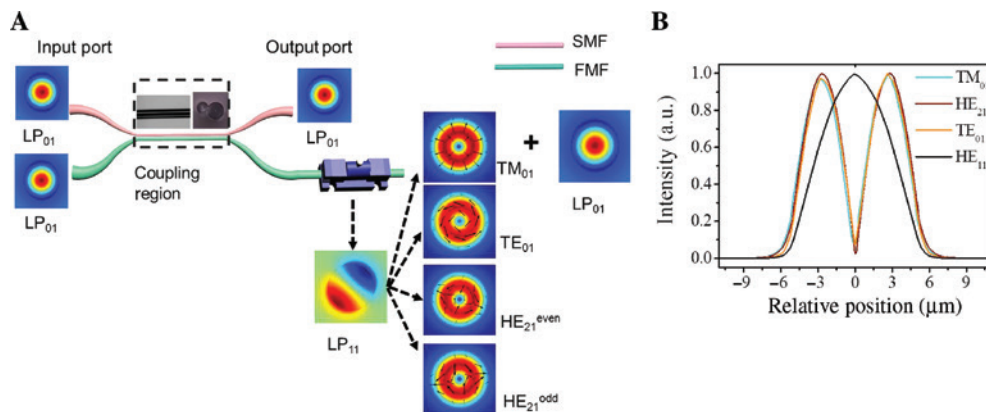
Figure 1: The structure and vector modes profiles of mode selective coupler.
(A) The schematic of the mode selective coupler. Inset: the top- and cross-sectional pictures of the coupling region. (B) Intensity profiles of vector modes in few-mode fiber based on numerical calculation.

radial polarization (TM_{01}), azimuthal polarization (TE_{01}), and hybrid polarization ($HE_{21}^{even/odd}$) states with donut-shaped intensity distribution. A polarization controller (PC) is added in the FMF to effectively eliminate the degeneracy of LP_{11} mode. According to the extrusion and rotation force of PC, the polarization distribution of vector modes can be changed, which leads to excite individual vector modes in different polarization states and forms vortex donut-shaped modes [5, 7, 18]. The vector modes intensity profiles are calculated as shown in Figure 1B, which have almost same effective propagating constants and energy distribution, and HE_{11} mode can be stably transmitted in the FMF, i.e. the light of LP_{01} mode propagates through the FMF (green) input port of the MSC and directly outputs at the FMF output port.

The mode conversion principle of the MSC is in accordance with phase matching condition between the fundamental mode in the SMF and the HOMs in the FMF based on the coupled-mode theory [30, 31]. Figure 2A is the mode effective indices dependent on the core radii and the horizontal dashed line indicates the phase matching point between HE_{21} mode of the FMF and LP_{01} (HE_{11}) mode of the SMF. When these modes in two fibers have the same

effective refractive index of 1.4525, the target core radius ratio between the SMF and FMF is valued around 0.558. In this case, the phase matching condition is satisfied, the core diameters of SMF/ FMF should be 5.58/10 μm, and the cladding diameters of SMF/FMF are 110/125 μm. Therefore, the asymmetric cladding diameters of SMF/FMF need different pre-tapering diameters of the SMF before fusing them together. Beam propagation simulation (Rsoft software, RSoft Design Group, Ossining, NY, USA) is used to show the mode evolution process of the asymmetric fused MSCs with the calculated fiber core ratios, as illustrated in Figure 2B. The light of LP_{01} mode in the input SMF is converted into LP_{11} mode in the FMF output port, meanwhile another LP_{01} mode at different wavelength is launched in the FMF input port. The simulation result proves that the LP_{11} and LP_{01} modes can be multiplexed at the FMF output port of the MSC.
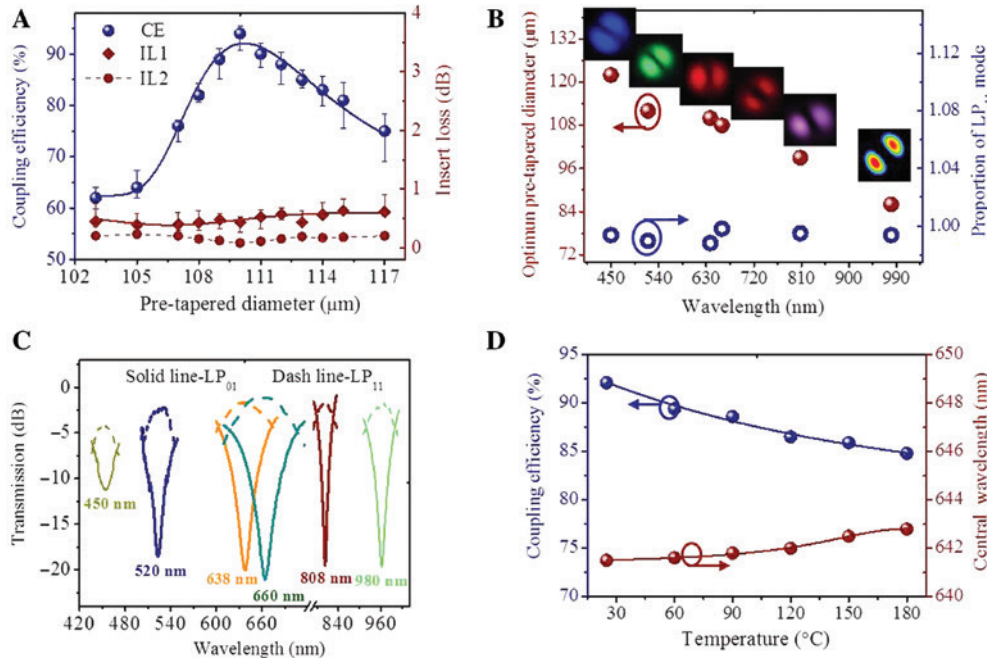
Conversion efficiency (CE) and insert loss (IL) are two pivotal factors for evaluating the MSC. CE is defined as the power ratio of the output LP_{11} mode and input LP_{01} mode, and IL1 and IL2 are the power ratios of the FMF output port to the SMF and FMF input ports, respectively. Figure 3A shows the CE and IL of 638 nm MSC with different pre-tapering diameters. The SMF cladding diameter is optimized around 110 μm for the best pre-tapering diameter before fusing with the FMF, which is consistent with the calculated ratio of the fiber core in Figure 2A. In this case, CE is as high as 94%, IL1 is about 0.5 dB, and IL2 is below 0.2 dB, the input light from SMF and FMF ports can almost be completely output by a MSC. Figure 3B displays the optimal pre-tapered cladding diameters and proportion of LP_{11} mode generated by the MSCs at different wavelengths, and the intensity distribution of lobe-shaped LP_{11} modes is monitored by charge coupled device (CCD) (Thorlabs, DCC1240C, Newton, NJ, USA) at corresponding wavelengths, as shown in the inset. Using the method of mode decomposition and reconstruction based on numerical analysis, the proportion of LP_{11} mode in the total output modes can be calculated [32], which are more than 98% indicating that these MSCs have exceedingly high LP_{11} mode purity.

The transmission spectra of the MSCs (450, 520, 638, 660, 808, and 980 nm) in the optimal pre-tapered cladding diameters are measured from the SMF and FMF output ports by using a broadband optical source (YSL Photonics SC-5, Wuhan, China) and an optical spectrum analyzer (Yokogawa, AQ6370D, Japan). The maximum transmission power of the LP_{11} mode for a 660 nm MSC is close to –1 dB, and the corresponding LP_{01} mode is attenuated below –21 dB, which shows that the high power extinction ratio provides high mode CE of LP_{11} mode. The 3-dB mode conversion bandwidth of the MSCs are 18, 9, 10, 12, 7, and 12 nm, respectively, as shown in
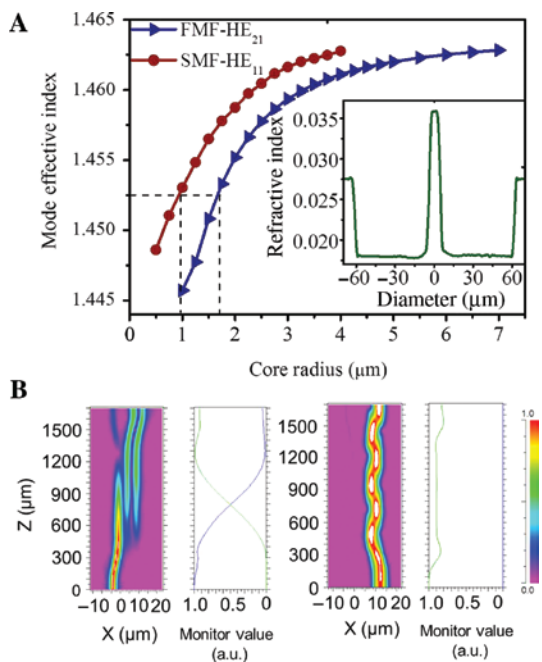
Figure 2: The numerical calculation and simulation of phase matching condition.
(A) The mode effective index curves for the LP_{01} and LP_{11} modes vs. core radius at the wavelength of 660 nm. Inset: refractive-index distribution of the few-mode fiber (FMF). (B) Power exchanging curves in the coupling region. LP_{01} mode is lunched in the input single mode fiber (SMF) port (left) and input FMF port (right), the blue and green lines show the power of SMF and FMF, respectively.

Figure 3: The performance of mode selective couplers (MSCs).
(A) Conversion efficiency and insertion loss of 638 nm MSC at different pre-tapered diameters of SMF. (B) Optimum pre-tapered cladding diameters and the proportion of LP_{11} mode of visible light MSCs. Inset: experimental LP_{11} mode intensity profiles of the all-fiber MSCs at 450, 520, 638, 660, 808, and 980 nm. (C) Transmission spectra of visible wavelength and 980 nm MSCs. (D) Conversion efficiency and central wavelength of 660 nm MSC heated from 25°C to 180°C.

Figure 3C. The result shows a broad bandwidth of the MSC; therefore, the pulsed beam with wide broadband could be converted to pure HOM. To investigate the performance of temperature variation, the 660 nm MSC is set in a thermostat and heated from 25°C to 180°C. It can be seen from Figure 3D that the CE has a slightly declining trend with increasing temperature, which is reduced by about 8%. The result may be caused by the gap between two fiber cores enlarged, so that the light transmitted in two fibers is partially leaked out. Nevertheless, the CE is still higher than 84.5% when the temperature is up to 180°C. Although the central wavelength of mode conversion is slightly red-shifted by 1.3 nm with the temperature increases, which can be ignored relative to the broad bandwidth of the MSC. The MSC as a mode converter overcomes the shortcoming of LPFG with highly susceptible to the temperature change.

3 Characterization analysis of donut beams

TM_{01}, TE_{01}, and $HE_{21}^{even/odd}$ beams are called CVBs and can stably propagate in the FMF, because these modes are eigenmodes with annular mode field intensity and

symmetric polarization distribution along with the optical axis. Controlling the pressure force of PC, the CVBs generated by 520 and 638 nm MSCs can detected by a CCD, as shown in Figure 4. Four vector beams have different polarization distribution across the donut-like beams, and a linear polarizer placed before the CCD is used to distinguish their polarization distribution. The first column is the near-field distribution of donut-like vector mode, and the later four columns are the transmitted intensity evolution with the rotating direction (marked by bidirectional arrow) of the linear polarizer, which indicates that the TM_{01}, TE_{01}, and HE_{21}^{even}, HE_{21}^{odd} are two pairs of orthogonal beams.
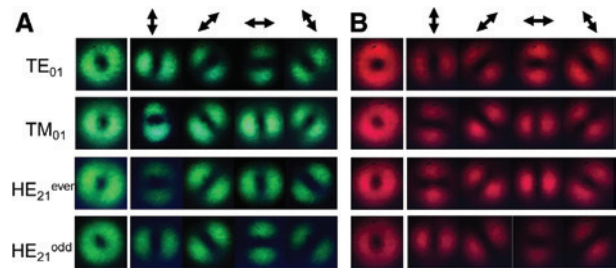
Figure 4: Polarization characteristic of cylindrical vector beams. Near-field intensity distribution of TM_{01}, TE_{01}, $HE_{21}^{even/odd}$ modes generated by all-fiber mode selective couplers at (A) 520 and (B) 638 nm.

MSCs generate CVBs by controlling the polarization modality of LP_{11} mode, while OVB carrying orbital angular momentum (OAM) can be obtained by adjusting phase property of LP_{11} mode. The phase of the OVB has a centrally symmetric spiral distribution, so the light field intensity around the central axis is zero and the phase is singular. There are two methods for generating the $OAM_{\pm1}$ modes, one method is the linear superposition of orthogonal vector eigenmodes HE_{21}^{even} (HE_{21}^{odd}) and TE_{01} (TM_{01}) with $\frac{\pi}{2}$ phase shift by adding and adjusting a PC at the fiber output port [8, 33], another is to convert CVB to OVB by using a quarter-plate and a linear polarizer [34, 35].

By adjusting the rotating angle and pressure of PC, a $\frac{\pi}{2}$ phase shift between two orthogonal vector modes is introduced, the first-order 808, 660, and 450 nm OVBs are generated from FMF output port of MSC by superposing the two vector modes as shown in Figure 5A–C. And another Gaussian beam from the SMF output port acts as an interference beam, the hand orientations of the OVBs are obtained based on the direction of interference fringes. The method of interference and reference beams output by a MSC not only eliminates the extra interference light source, but also

ensures the same frequency of the two beams, which is beneficial to the interference operation. The counter-clockwise (a3, b3, c3) and clockwise (a4, b4, c4) spiral interferograms represent that the topological charges are +1 and –1, respectively. A polarizer is added before the CCD to verify whether these OVBs are circular-polarization OAMs (CP-OAMs) or linear polarization OAMs. The results in Figure 5D show that these OVBs are CP-OAMs, because the CP-OAM has almost equal intensity distribution as rotating the polarization direction of the polarizer [35].

4 All-fiber donut beams multiplexing scheme and application

By optimizing the parameters of the MSCs, the wavelength-dependent donut beams are produced and multiplexed by Gaussian beams with different wavelengths, which are output from a common FMF and concentrically distributed, as shown in Figure 6A. The scheme is very desired and expected for multicolor STED nanoscopy, which requires a single STED beam with donut intensity
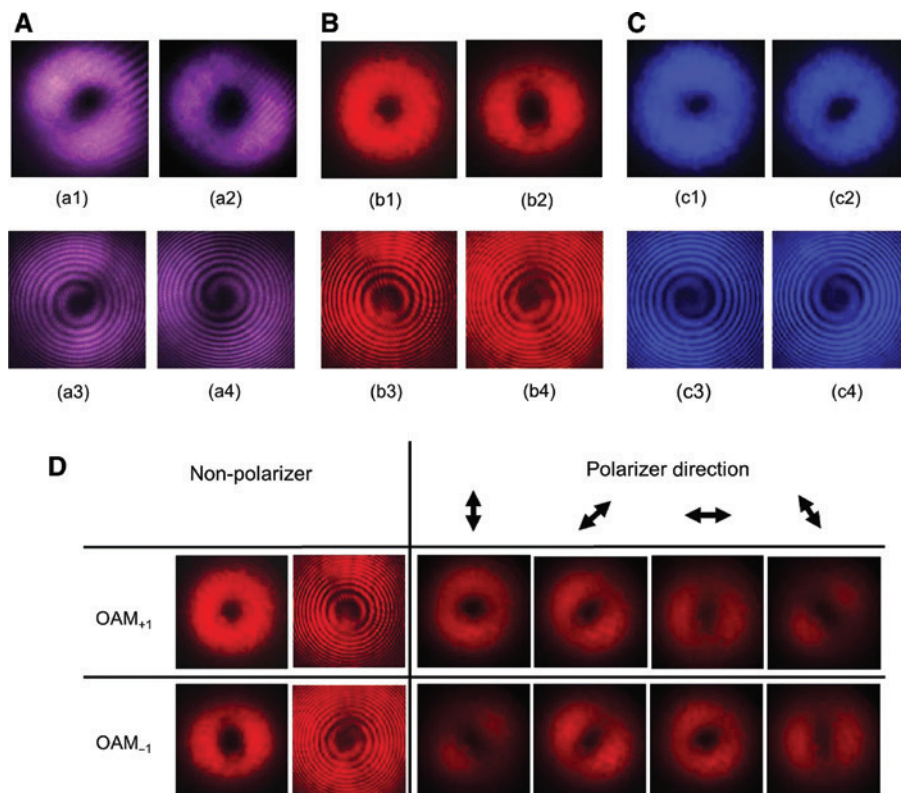
Figure 5: Near-field intensity distribution of vortex beams.
The orbital angular momentums (OAMs) output by (A) 808, (B) 660, and (C) 450 nm mode selective couplers, the donut-shaped intensities (a1, a2), (b1, b2), (c1, c2) and their spiral interferences (a3, a4), (b3, b4), (c1, c2). (D) Near-field intensity distribution of 660 nm OAMs.
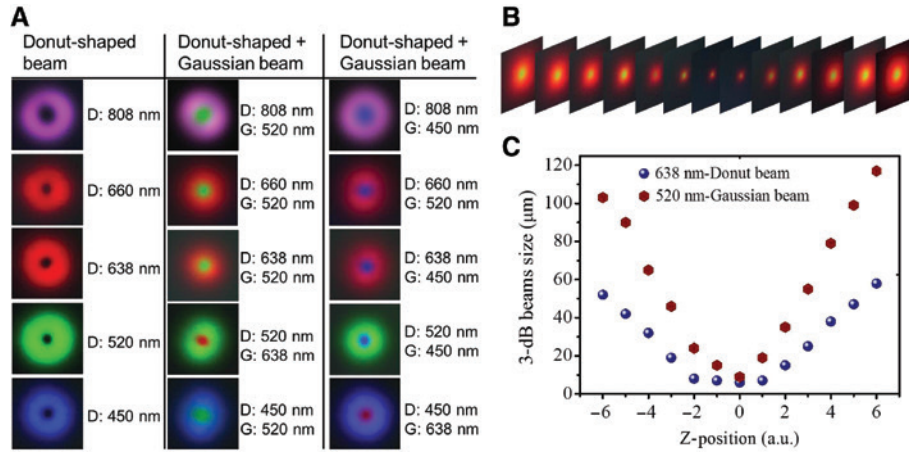
Figure 6: The characteristics of the multiplexed beams.
(A) Intensity distribution of two color beams are multiplexed with flexible wavelengths. D and G refer to donut- and Gaussian-shaped beams, respectively. (B) Three-dimensional intensity distribution of donut/ Gaussian beams (638 nm/ 520 nm). (C) Beam sizes of the multiplexed beams at different positions before and after the focus of the lens.

and multiwavelength Gaussian excitation spots in the focal region [36].

Through recording beam profiles horizontally at the same height before and after lens focus, three-dimensional intensity slices and 3-dB spot sizes of donut/excitation beams are shown in Figure 6B, C. The smallest beam spots of donut and Gaussian are obtained at the lens focus, which are in the same position. Around the lens focal points, the beam waists are enlarging along with the direction of light transmission (along Z position) and the shapes of these beams are identical. As the donut and Gaussian beams are delivered from the same fiber, they are self-aligned in any position. The results indicate that the MSCs can not only convert the LP_{01} mode to a donut-shaped beam at the desired wavelength, but also multiplex other color fundamental mode. The MSCs have the advantage of strictly self-aligned beams in fiber.

To integrate the donut beam produced by MSC can be a compact and convenient optical source for STED microscopy, an all-fiber MSC multiplexing mechanism combined by a confocal microscope system is designed, as shown in Figure 7. LD1 and LD2 are displayed as visible laser sources. The donut beam generated by the MSC is transmitted to the sample on the focal plane of the objective (1.4 NA, oil-immersion, Nikon, Tokyo, Japan). Through scanning a single gold nanoparticle (Abberior, 150-nm, Gottingen, Germany), the reflected light is collected through a multimode fiber of 50 μm core diameter, which is equivalent to a pin hole at the confocal plane, and detected by an avalanche photodiode photon counter (Excelitas, SPCM-AQRH-14-FC, Fremont, CA, USA). The power ratio between the SMF and the FMF output ports is monitored by a power

meter (Thorlabs, PM100D, Newton, NJ, USA) and the mode intensity distribution is detected by CCD.

The STED wavelength is usually selected at the longer wavelength tail of the emission spectrum [37]. Therefore, in order to preliminarily verify the extinction effect, the combination of STED/excitation wavelength in the experiment is 638 nm/520 nm. Point spread function (PSF), as profiles function of objective focal plane of donut and excitation beams, determines the STED microscope resolution and is very important for building and further developing STED microscopy [16]. The HE_{21} mode has the lowest centrally residual energy and even-intensity distribution according to the intensity profiles in Figure 8A; therefore,
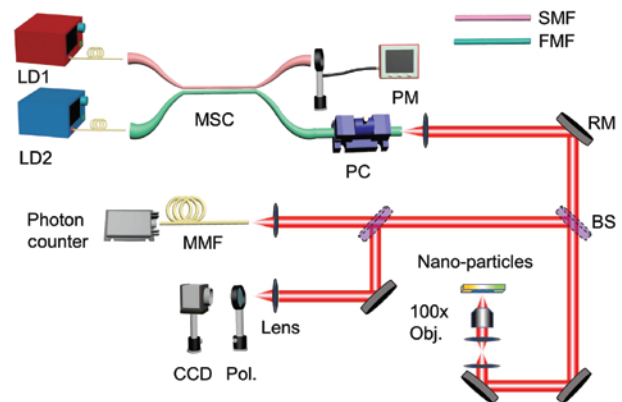
Figure 7: Confocal microscope system for multiplexing and detecting donut and Gaussian beams.
LD, laser diode; PM, power meter; PC, polarization controller; Lens, double-glued lens; RM, reflection mirror; Obj., objective lens; BS, beam splitter; Pol., linear polarizer; CCD, charge coupled device; MMF, multimode fiber.
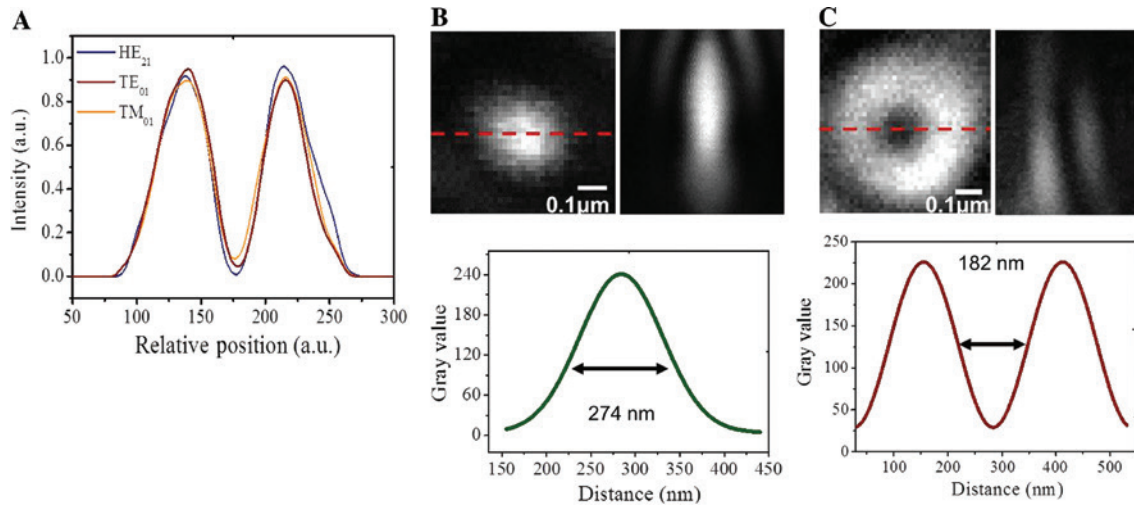
Figure 8: Point spread function of donut and Gaussian beams.
(A) Experimentally measured mode field intensity curves of TE_{01}, TM_{01}, and HE_{21} modes. The confocal intensity distribution on the (left) cross- and (right) axial-sections, and the line profiles of the cross-section of (B) Gaussian and (C) donut beams.

the HE_{21} mode is considered as a STED beam. Figure 8B, C shows the confocal intensity distribution of donut and Gaussian beams on the cross- and axial-sections. The fitted full width at half maximum (FWHM) curve of the excitation PSF is about 274 nm, and the donut FWHM is around 182 nm, the extinction ratio between the center and peak value is 10 dB, having the effect of erasing the excitation beam. Because of the self-alignment and extinction performance, the fiber-based multiplexing scheme acting as an optical source for STED microscopy has significant advantages over conventional two-beam spatial alignment configuration. It can greatly enhance the system robustness against vibration and environmental turbulence, and ease the requirement for STED system installation.

5 Discussion

The self-alignment characteristic of donut and Gaussian beams propagating in a common fiber has been successfully demonstrated for STED imaging [15, 16]. Here the all-fiber MSC-based mechanism is proposed to generate donut beams and deliver two beams from a FMF at the same time, which can be potentially applied in STED microscopy. There are two important factors determining the quality of the donut-shaped beam, one is the centrally zero intensity of donut beam, which is critical for the imaging resolution of STED microscopy, another is that the mode CE should be high enough to assure the mode purity. When the LP_{01} mode is converted to LP_{11} mode, if phase match condition

is not strictly satisfied, the unconverted LP_{01} mode is also coupled in the MSC, which increases the dark hollow intensity of the donut beam. The quality of the donut beam can be further improved by optimizing the structure of the FMF, as the dark hollow intensity is determined by the purity of eigenvector modes as shown in Figure 1B. Yan et al. designed a vortex fiber with ring-shaped high refractive index profile which can propagate OAM state stably [16]. Heng et al. proposed a graded-index fiber to break the degeneracy of vector modes within a mode group [38]. These fibers are characterized by a high refractive index difference between the core and cladding, which is guaranteed to separate HE_{21} mode from TM_{01} and TE_{01} modes.

For example, we simulate the intensity profiles of HE_{21} and HE_{11} modes by using step-index and graded-index fibers with the same core radius (5 μm) and Δn (0.04)

$$\left(n(r) = n_{\text{cladding}} + \Delta n \times \left(1 - \frac{r}{r_{\text{core}}} \right)^{\alpha} \right.,$$ (Δn: the refractive index

difference between the core and cladding, α: the shape factor), as shown in Figure 9A. The 3-dB aperture of HE_{21} mode in graded-index fiber is less than that of the step-index fiber (~2 μm), and has a lower central hollow intensity (0.98%) than step-index fiber (3.6%). Moreover, using the same Δn (0.04), the 3-dB aperture of HE_{21} mode at different core radii and the effective refractive index difference (Δn_{eff}) of vector modes are shown in Figure 9B, C. The calculated results indicate that the small fiber core radius has a relatively narrow 3-dB aperture of HE_{21} mode and a large Δn_{eff} with TE_{01}/TM_{01} modes. Therefore, an optimized refractive index profile of the FMF in the MSC can decline
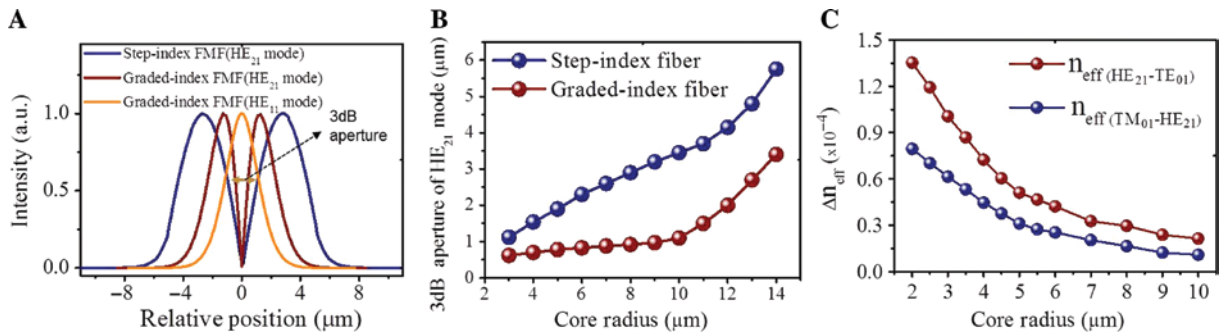
Figure 9: Comparison of step-index and graded-index fibers.
(A) Intensity profiles of HE_{21} and HE_{11} modes in a step-index and graded-index few-mode fiber (FMF) based on numerical calculation. (B) The 3-dB aperture of HE_{21} mode as a function of FMF core radius. (C) Δn_{eff} of vector modes vs. the core radius in a graded-index FMF.

the dark hollow intensity of the STED beam and erase the area of the excitation beam to a greater extent, which can improve the extinction ratio of STED microscopy.

Additionally, Mao et al. proposed some vortex beam generators based on LPFG and fiber taper, and combining with mode-locked fiber laser to generate several picoseconds pulse, which was used for manipulating nanosheets. The narrow transmission spectrum of the LPFG effectively implemented filter; however, mode coupling efficiency of the LPFG was easily affected by external pressure, resulting in instability of HOMs [39]. As for the MSC which shows a broad mode conversion bandwidth, a high mode purity exists in the available transmission spectrum. In this case, the pulsed STED beam could be transformed into stable HOM, while other devices such as LPFG and AIFG can only support narrow bandwidth STED beam. When using a MSC inside the STED microscopy, the MSC functions as both a mode converter and multiplexer for generating and combining donut and Gaussian beams, no extra WDM is needed to simplify the confocal setup. Therefore, the MSC with robust characteristics potentially provides optical source for STED microscopy.

which can also be multiplexed. The PSF of donut beam measured by confocal system shows the 10-dB extinction ratio. In the next work, we will optimize the structure of the FMF, and employ the multiplexing scheme to verify the imaging resolution of the STED microscope system by using the fluorescent-labeled specimen. The proposed scheme can solve several technical problems of generating visible donut beam in high-cost and complicated system, which provides a novel method for constructing optical source in STED microscope system.

6 Conclusion

In summary, we demonstrate a compact and stable generator and multiplexer of donut-shaped beam based on the all-fiber MSC at visible wavelength. An asymmetric fused MSC converts the fundamental mode to HOMs, which has the advantage of more than 7-nm mode conversion bandwidth (3-dB), the efficiency of the fundamental mode to LP_{11} mode of 94%, the loss of less than 0.5-dB, and LP_{11} mode purity of over 98%. The donut-shaped CVBs and CP-OVBs are generated by controlling the polarization and phase of the HOMs, respectively. Any wavelength beams respectively enter two input ports of the MSC,

References

[1] Li A, Ye J, Chen X, Shieh W. Fabrication of a low-loss fused fiber spatial-mode coupler for few-mode transmission. IEEE Photonic Technol Lett 2013;25:1985–8.

[2] Gasulla I, Kahn JM. Performance of direct-detection mode-group-division multiplexing using fused fiber couplers. J Lightwave Technol 2015;33:1748–60.

[3] Li A, Al Amin A, Chen X, Shieh W. Transmission of 107-Gb/s mode and polarization multiplexed CO-OFDM signal over a two-mode fiber. Opt Express 2011;19:8808–14.

[4] Ren F, Li J, Wu Z, et al. All-fiber optical mode switching based on cascaded mode selective couplers for short-reach MDM networks. Opt Engng 2017;56:046104.

[5] Wang F, Shi F, Wang T, Pang F, Wang T, Zeng X. Method of generating femtosecond cylindrical vector beams using broadband mode converter. IEEE Photonic Technol Lett 2017;29:747–50.

[6] Wang T, Yang A, Shi F, Huang Y, Wen J, Zeng X. High-order mode lasing in all-FMF laser cavities. Photonics Res 2019;7:42–9.

[7] Huang Y, Shi F, Wang T, et al. High-order mode Yb-doped fiber lasers based on mode-selective couplers. Opt Express 2018;26:19171–81.

[8] Wang T, Wang F, Shi F, et al. Generation of femtosecond optical vortex beams in all-fiber mode-locked fiber laser using mode selective coupler. J Lightwave Technol 2017;35:2161–6.

[9] Shi F, Cheng P, Huang Y, et al. Mode-locked all-fiber laser emitting two-color high-order transverse mode. IEEE Photonic Technol Lett 2019;31:497–500.

[10] Zou J, Wang H, Li W, et al. Visible-wavelength all-fiber vortex laser. IEEE Photonic Technol Lett 2019;31:1487–90.

[11] Wang X, Wang D, Shen X, et al. Supercontinuum generation from ultraviolet and visible wavelength based on the higher-order modes of photonic crystal fiber. Optik 2017;140:423–6.

[12] Oubei HM, Duran JR, Janjua B, et al. 4.8 Gbit/s 16-QAM-OFDM transmission based on compact 450-nm laser for underwater wireless optical communication. Opt Express 2015;23:23302–9.

[13] Zhao Y, Wang J. High-base vector beam encoding/decoding for visible-light communications. Opt Lett 2015;40:4843–6.

[14] Hell SW, Wichmann J. Breaking the diffraction resolution limit by stimulated emission: stimulated-emission-depletion fluorescence microscopy. Opt Lett 1994;19:780–2.

[15] Gu M, Kang H, Li X. Breaking the diffraction-limited resolution barrier in fiber-optical two-photon fluorescence endoscopy by an azimuthally-polarized beam. Sci Rep 2014;4:3627.

[16] Yan L, Kristensen P, Ramachandran S. Vortex fibers for STED microscopy. Appl Phys Lett Photon 2019;4:022903.

[17] Zhan Q. Cylindrical vector beams: from mathematical concepts to applications. Adv Opt Photonics 2009;1:1–57.

[18] Yao S, Ren G, Shen Y, Jiang Y, Zhu B, Jian S. Tunable orbital angular momentum generation using all-fiber fused coupler. IEEE Photonic Technol Lett 2017;30:99–102.

[19] Novotny L, Beversluis MR, Youngworth KS, Brown TG. Longitudinal field modes probed by single molecules. Phys Rev Lett 2001;86:5251.

[20] Kawauchi H, Yonezawa K, Kozawa Y, Sato S. Calculation of optical trapping forces on a dielectric sphere in the ray optics regime produced by a radially polarized laser beam. Opt Lett 2007;32:1839–41.

[21] Aasen H, Honkavaara E, Lucieer A, Zarco-Tejada PJ. Quantitative remote sensing at ultra-high resolution with UAV spectroscopy: a review of sensor technology, measurement procedures, and data correction workflows. Remote Sens 2018;10:1091.

[22] Milione G, Wang T, Han J, Bai L. Remotely sensing an object's rotational orientation using the orbital angular momentum of light. Chin Opt Lett 2017;15:030012.

[23] Ramachandran S, Kristensen P. Optical vortices in fiber. Nanophotonics 2013;2:455–74.

[24] Zhou R, Haus JW, Powers PE, Zhan Q. Vectorial fiber laser using intracavity axial birefringence. Opt Express 2010;18:10839–47.

[25] Piccirillo B, D'Ambrosio V, Slussarenko S, Marrucci L, Santamato E. Photon spin-to-orbital angular momentum conversion via an electrically tunable q-plate. Appl Phys Lett 2010;97:241104.

[26] Wang B, Shi J, Zhang T, Xu X, Cao Y, Li X. Improved lateral resolution with an annular vortex depletion beam in STED microscopy. Opt Lett 2017;42:4885–8.

[27] Zhou Z, Tan Q, Jin G. Cylindrically polarized vortex beams generated by subwavelength concentric Al metallic gratings. J Optics 2011;13:075004.

[28] Terhalle B, Langner A, Päivänranta B, Guzenko VA, David C, Ekinci Y. Generation of extreme ultraviolet vortex beams using computer generated holograms. Opt Lett 2011;36:4143–5.

[29] Zhang W, Huang L, Wei K, Li P, et al. High-order optical vortex generation in a few-mode fiber via cascaded acoustically driven vector mode conversion. Opt Lett 2016;41:5082–5.

[30] Ismaeel R, Lee T, Oduro B, Jung Y, Brambilla G. All-fiber fused directional coupler for highly efficient spatial mode conversion. Opt Express 2014;22:11610–9.

[31] Riesen N, Love JD. Weakly-guiding mode-selective fiber couplers. IEEE J Quantum Electron 2012;48:941–5.

[32] Huang L, Guo S, Leng J, Lü H, Zhou P. Real-time mode decomposition for few-mode fiber based on numerical method. Opt Express 2015;23:4620–9.

[33] Li S, Mo Q, Hu X, Du C, Wang J. Controllable all-fiber orbital angular momentum mode converter. Opt Lett 2015;40:4376–9.

[34] Han Y, Chen L, Liu YG, et al. Orbital angular momentum transition of light using a cylindrical vector beam. Opt Lett 2018;43:2146–9.

[35] Mao B, Liu Y, Zhang H, et al. Complex analysis between CV modes and OAM modes in fiber systems. Nanophotonics 2018;8:271–85.

[36] Sidenstein SC, D'Este E, Böhm MJ, Danzl JG, Belov VN, Hell SW. Multicolour multilevel STED nanoscopy of actin/spectrin organization at synapses. Sci Rep 2016;6:1–8.

[37] Ronzitti E, Harke B, Diaspro A. Frequency dependent detection in a STED microscope using modulated excitation light. Opt Express 2013;21:210–9.

[38] Heng X, Gan J, Zhang Z, et al. All-fiber stable orbital angular momentum beam generation and propagation. Opt Express 2018;26:17429–36.

[39] Mao D, Li M, He Z, et al. Optical vortex fiber laser based on modulation of transverse modes in two mode fiber. Appl Phys Lett Photon 2019;4:060801.